ADVANCED FUNCTIONAL MATERIALS

FULL PAPER

DOI: 10.1002/adfm.200500667

Formation of Silver Nanoprisms with Surface Plasmons at Communication Wavelengths**

By *Vytautas Bastys*, *Isabel Pastoriza-Santos*,* *Benito Rodríguez-González*, *Rimas Vaisnoras*, and *Luis M. Liz-Marzán**

Silver nanoprisms with strong absorption in the near-IR have been synthesized using a modification of the photoinduced method by illuminating preformed silver seeds under different illumination conditions. Low-intensity light-emitting diodes and white light combined with different color filters are used as light sources. The lateral dimensions of the nanoprisms are found to be correlated in a quasilinear fashion with the emission wavelength and the position of the main in-plane dipole plasmon band. The structural characterization of the Ag nanoparticles, carried out using scanning electron microscopy, transmission electron microscopy (TEM), high-resolution TEM, and electron diffraction, reveal that the particles are flat and have a single-crystal face-centered-cubic structure. Time-resolved studies suggest that the nanoprisms are formed by steady consumption of the original Ag seeds with little variation of the aspect ratio after a short induction time.

1. Introduction

Nanotechnology promises to provide solutions for and tools with which to tackle existing difficulties and forthcoming challenges.[1] While "physical nanotechnologies", such as electron-beam lithography, are widely applied in micro- and nanoelectronics, nanoparticle-based technologies are more rare and mostly restricted to biological applications.[2] Metal nanoparticles are among the most promising systems for applications in optics and electronics mainly because of their characteristic large electric-field enhancement, which is directly linked to surface plasmons arising from the resonance of the conduction electrons of individual nanoparticles upon interaction with an incoming electromagnetic field.[3] The plasmon-resonance conditions depend on a number of parameters, such as particle size, surface charge, the nature of the dielectric environment, and interparticle coupling, but the particle morphology has been shown to play a fundamental role.[4] Applications of metal nanoparticles in sensors,[5] plasmonic devices,[6] and surface-enhanced Raman spectroscopy (SERS)[4a,b,7] are already well established. Since the formation of anisotropic nanoparticles also provides a convenient tool to control the optical response, mainly through variation of the aspect ratio,[4b–e,8] new methods to produce disks,[9] rods and wires,[10] and prisms[11–13] have been rapidly developed in the last few years.

Recent publications have focused on the synthesis and optical characterization of gold[11] and silver[12,13] nanoprisms because of their unusual optical properties, which result in surface-plasmon resonance (SPR) peaks at relatively long wavelengths.[13a] Focusing on silver, various physical and chemical procedures have been devised to fabricate nanoprisms. A good example of an effective physical technique to prepare Ag nanoprisms is nanosphere lithography (NSL).[14] This lithographic approach yields nanoparticles supported on solid substrates and is capable of producing Ag nanoprisms with good control over their morphology, and even of fabricating large arrays of well-ordered nanoparticle structures. Although these lithographic nanofabrication techniques have been demonstrated to be an alternative to solution-phase methods, the chemical methods are more versatile. So far, two main chemical approaches can be identified: chemical reduction of metal salts[12] and photoinduced aggregation of small nanoparticle seeds.[13] The latter has recently become very popular, especially in the case of silver. Callegari et al.[13b] first demonstrated that the use of filters during illumination directly influences the final geometry of the nanoprisms. In a detailed mechanistic study, Jin et al.[13c] have recently proposed that the process is mainly controlled by the charge distribution on the seeds so that, while aggregation is induced by illumination with a laser beam of a certain wavelength, further growth could be prevented by illumination with a secondary laser tuned to the quadrupole resonance of the intermediate species. In these studies the obtained plasmon resonances could be tuned between approximately 400 and 1000 nm, but well-defined plasmons at lower energies (longer wavelengths) have not been reported so far, despite the great interest they could raise if the communication wave-

[*] Dr. I. Pastoriza-Santos, Prof. L. M. Liz-Marzán, B. Rodríguez-González
Departamento de Química Física, Universidade de Vigo
36310 Vigo (Spain)
E-mail: pastoriza@uvigo.es; lmarzan@uvigo.es
V. Bastys, Prof. R. Vaisnoras
Faculty of Physics and Technology, Vilnius Pedagogical University
Studentu St. 39, 08106 Vilnius (Lithuania)

[**] Support from the Spanish Ministerio de Educación y Ciencia/FEDER (Project MAT2004-02991) is gratefully acknowledged. The authors thank Dr. Jorge Pérez-Juste and Prof. Paul Mulvaney for helpful discussions. Supporting Information is available online from Wiley InterScience or from the author.

ADVANCED FUNCTIONAL MATERIALS

length (1550 nm) could be matched. Nanoparticles with large absorption coefficients around 1.55 μm could be used, for instance, to coat communication fibers and, thereby, reduce losses that are responsible for signal contamination. Apart from this obvious application, other fields where such systems would become useful are biotechnology, since they could allow local heating with low-energy irradiation,[15] and glazing for the selective attenuation of IR solar radiation.[16]

In this paper, we present a modification of the photoinduced method, using either low-intensity light-emitting diodes (LEDs) of different emission wavelengths or white light combined with different color filters for illumination; this allows the preparation of Ag nanoprisms with high aspect ratios, so that the in-plane dipole plasmon resonance is shifted to wavelengths above 1 μm. We additionally discuss the structural and optical properties of the obtained Ag nanoprisms using (scanning and transmission) electron microscopy techniques and UV–vis–near-IR (UV–vis–NIR) spectroscopy. Finally, we propose a mechanism for the formation of the nanoparticles on the basis of time-resolved optical measurements.

2. Results and Discussion

2.1. Growth of Nanoprisms via LED Illumination

Ag nanoprisms were grown using a modification of the photoinduced method[8] through illumination of a preformed Ag-seed solution using low-intensity LEDs with different emission spectra. Specifically, we used LEDs with emission bands centered at 518 nm (hereafter referred to as green LEDs), 641 nm (hereafter red1 LEDs), and 653 nm (hereafter red2 LEDs) (see spectra below). The minimum luminous intensities and the viewing angles of the green and red LEDs, as well as the current applied in each experiment are indicated in Table 1.

The main difference in the results presented here with respect to previous photoinduced synthesis methods is the possibility to prepare silver nanoprisms with high absorption coefficients well within the NIR region. Callegari et al.[13b] selected their illumination wavelength by fitting colored filters in front of a conventional fluorescent tube, while Jin et al.[13c] used single-wavelength lasers for illumination, obtaining silver nanoprisms with varying sizes and plasmon resonances that could be tuned between approximately 400 and 1000 nm. Although Ag nanoprisms with plasmons at lower energies have not been reported so far, we found that illumination of an aqueous solution of spherical silver nanoparticles (average diameter 5.3 ± 1.5 nm, see Supporting Information and transmission electron microscopy (TEM) images below) with low-intensity LEDs leads to silver nanoprisms with high aspect ratios, so that the in-plane dipole plasmon resonance is red-shifted to wavelengths well above 1 μm (see Fig. 1). We start with a general description of the spectra, based on two representative samples made by illumination with green and red LEDs, which display main absorption bands at 1037 and 1491 nm, respectively. Since the main absorption band of the sample grown with red LEDs is centered at 1491 nm, prior to measurement of the spectrum it was necessary to exchange the solvent from water to D_2O via various centrifugation/redispersion cycles, so as to avoid overlap with the intense stretching vibrational peak of water at 1470 nm. Because above 1500 nm the absorption coefficient of D_2O increases dramatically (see Supporting Information), a shoulder still arises on the low-energy side of the plasmon band.

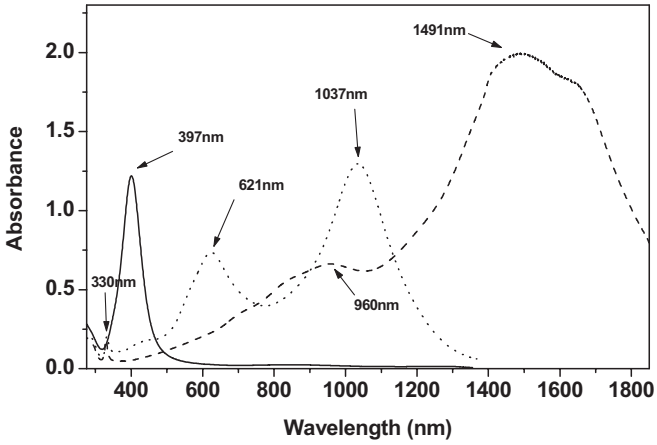

Figure 1. UV–vis–NIR spectra of dispersions of Ag seeds (–), and nanoprisms grown by illumination with green (·····) and red (red2, – – –) LEDs, in water and D_2O, respectively. The wavelengths of the corresponding maxima are indicated by the labels.

Besides the above-mentioned, intense, low-energy band, which is due to the in-plane dipole plasmon resonance associated with polarization of the conduction electrons in the plane parallel to the flat nanoprism, the spectra also display other bands, which is consistent with previously reported experimental and theoretical spectra.[4] Less-intense bands centered at 960 and 621 nm for the samples illuminated with red and green LEDs, respectively, most likely arise from the in-plane dipole resonance of a second population of smaller nanoprisms (see TEM images below), probably overlapping with the out-of-plane dipole (associated with polarization of the conduction electrons perpendicular to the plane of the nanoprisms) and in-plane quadrupole resonances of the larger ones. The relative intensity of this second band is larger for the sample illuminated with green LEDs, which may be related to the relative contribution of each population, owing to both the respective number of particles and extinction coefficients (which increases with particle size). Another well-defined peak (with

Table 1. Minimum luminous intensities and viewing angles of the green and red LEDs. The current applied in each experiment is also indicated.

Illumination source	Minimum luminous intensity [mcd]	Viewing angle [degrees]	Applied current [mA]
Green LEDs	7200	23	5
Red LEDs (red1)	10 000	6	20
Red LEDs (red2)	4500	10	30

low intensity) located (for both samples) at 330 nm is due to out-of-plane quadrupole resonances. This band has been predicted (mainly using discrete dipole approximation (DDA) calculations) to be independent of lateral size, but to undergo a slight red-shift when either the truncation degree increases or the aspect ratio decreases.[4d]

Compared with previous reports,[13c,d] our results confirm that illumination with higher emission wavelengths leads to formation of dispersions with longer in-plane plasmon wavelengths (621 and 1037 nm for an illumination wavelength of 518 nm; 960 and 1490 nm for an illumination wavelength of 653 nm, Fig. 1). Furthermore, the extinction spectrum of the nanoprisms is also sensitive to the aspect ratio of the particles, as well as to the truncation of the triangular nanoparticles;[4] thus, if we compare particles with the same thickness and assume no truncation, longer-wavelength peaks would correspond to longer sides (higher aspect ratios). As discussed in the following section, the thickness of the triangles was found to be independent of the irradiation wavelength. We can thus postulate that the side length of the particles is controlled by the irradiation wavelength.

2.2. Morphology and Structural Characterization

Characterization of the Ag-seed solution by high-resolution TEM (HRTEM) revealed that the colloid is constituted of tiny spherical particles 5.35 ± 1.53 nm in diameter (Fig. 2a and Supporting Information). Although we found that most of the particles have single-crystal face-centered-cubic (fcc) structures (Fig. 2c), there was also a very small fraction of particles with multitwinned structures (Fig. 2b).

Shown in Figure 3 are representative TEM images of the Ag nanoprism samples whose absorption spectra are displayed in Figure 1. Analysis of the TEM images yields average lateral dimensions of the nanoprisms made by illumination with green

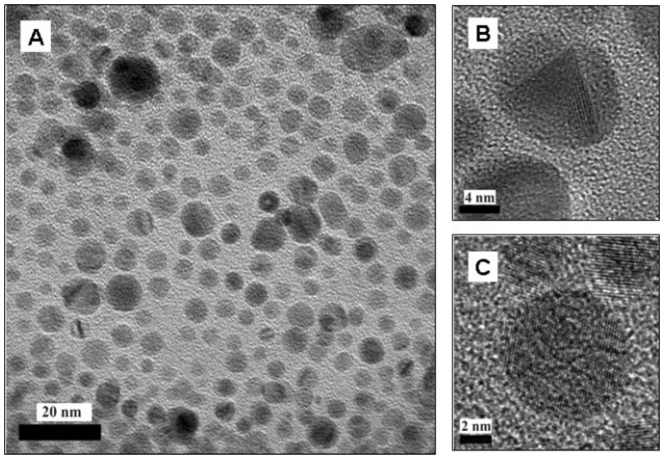

Figure 2. A) Representative TEM image of Ag seeds prepared by reduction of $AgNO_3$ with $NaBH_4$ in the presence of sodium citrate and poly(vinylpyrrolidone) (PVP). HRTEM images of a B) multitwinned and C) single-crystal Ag nanoparticle.

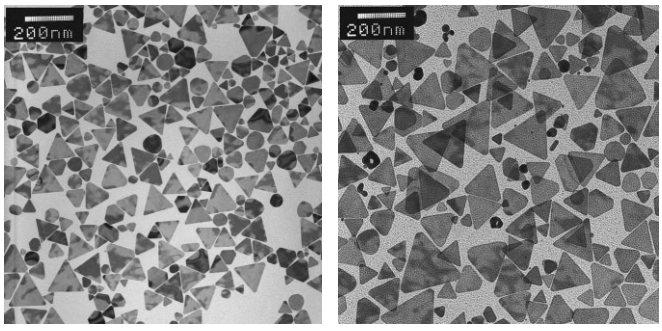

Figure 3. Representative TEM images of Ag nanoprisms prepared by illumination of Ag seeds with green (left) and red (red2, right) LEDs.

LEDs of 110 ± 16.5 nm, while illumination with red2 LEDs yields particles with an average side length of 242 ± 52.5 nm. The average lateral dimensions were determined by averaging over more than one hundred particles, neglecting a second smaller population since it was considered that, in spite of some polydispersity, there is a main population of larger particles that ultimately dominates the optical response of the dispersion. However, especially in the case of green LEDs, the second population (side length of 51 ± 8.5 nm) is not insignificant, and this is consistent with the larger relative intensity of the second band (621 nm) in the spectrum. Additionally, a small population of truncated nanoprisms is also present, which may be responsible for the presence of intermediate resonances between the quadrupolar out-of-plane and dipolar in-plane resonances.

Detailed scanning electron microscopy (SEM) analysis allowed us to measure the thickness, while categorically demonstrating the flat nature of the Ag nanoprisms (Fig. 4). The measurements were performed using holey Formvar polymer-coated copper grids as substrates for the deposition of concentrated nanoprism dispersions. Occasionally this led, in certain areas, to stacking of the nanoprisms perpendicular to the grid. From the SEM images, an average thickness of 10.5 ± 1.8 nm was obtained after subtraction of the thickness of the polymer (polyvinylpyrrolidone (PVP)) layers observed between the prisms. One should note here that the stacks are made of triangles with a variety of lateral dimensions, and still the obtained thickness shows a remarkably narrow distribution. Analysis of samples synthesized under different illumination conditions yield very similar average thickness values. Occasionally, bending of some nanoprisms was observed, which points to some structural instability of these nano-objects. A more detailed study of these observations will be reported elsewhere.

Further characterization of silver nanoprisms obtained using LEDs and filters was carried out by HRTEM. Figure 5 shows high-resolution images, as well as the corresponding electron diffraction pattern obtained from a single Ag nanoprism lying flat on the support film, with the electron beam perpendicular to the {111} main face, which reveals a regular, hexagonal, diffraction-spot array (Fig. 5b). Detailed analysis of the diffraction pattern shows that it corresponds to a [111] zone-axis single crystal with an atomically flat surface. Moreover the

ADVANCED FUNCTIONAL MATERIALS

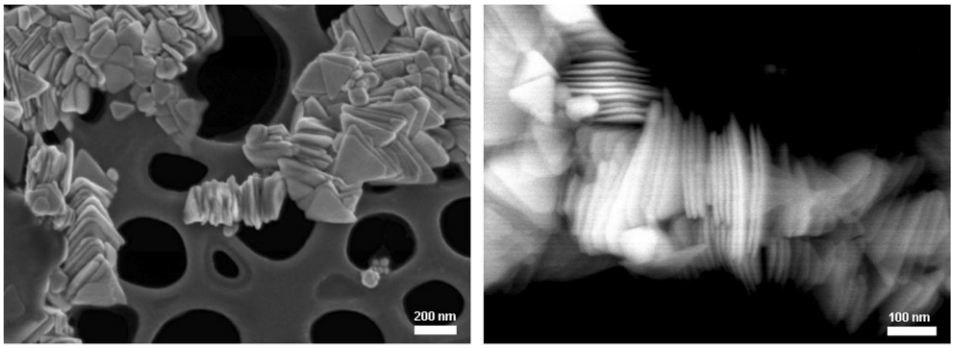

Figure 4. SEM images of silver nanoprisms made by illumination with red LEDs, stacked on a TEM grid, using both secondary electron imaging (SEI; left) and backscattered electron imaging (yttrium aluminum garnet (YAG) detector; right).

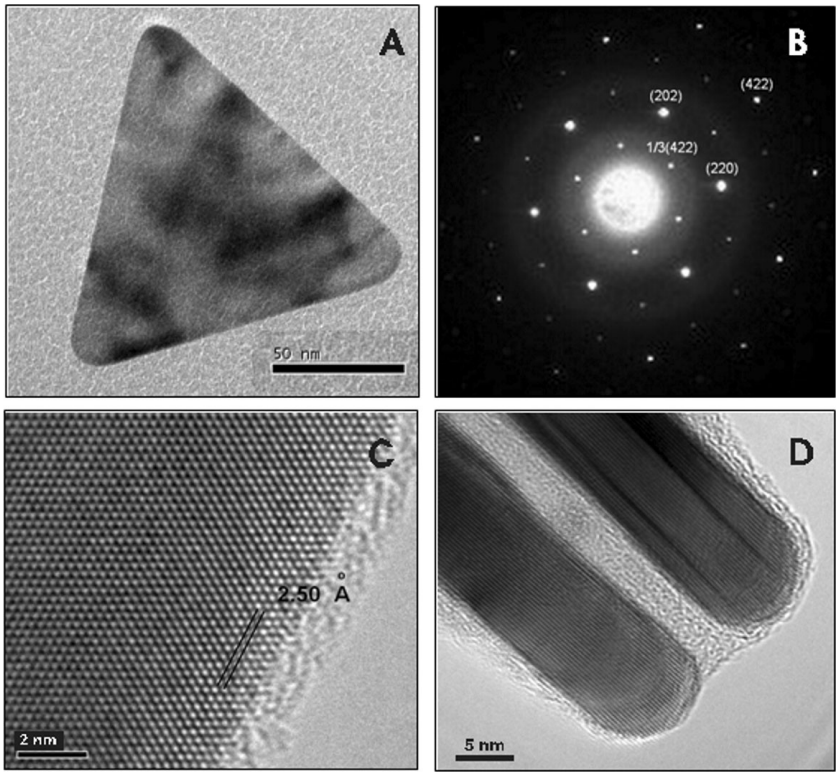

Figure 5. A) TEM image of a silver nanoprism. B) Electron diffraction pattern taken from an individual silver nanoprism and the assigned reflection indices. C) High-resolution lattice image with a spacing of 2.5 Å shown in the border of one of the main faces. D) High-resolution image of two Ag nanoprisms that are on their sides. The PVP-protected thin layer around the Ag nanoparticles can be seen.

pattern also displays interesting 1/3{422}-type faint spots, which are forbidden in a typical fcc single-crystal structure. Although the origin of these spots is not completely clear, some authors claim that they derive from a local hexagonal-like structure observable only for silver or gold samples that are atomically flat.[13a,f,17] Lofton et al.[18] recently proposed the presence of twinning planes in the platelets to explain the presence of these 1/3{422} forbidden spots, but we have not observed any acute edges in our TEM observations, as suggested by these authors.

The high-resolution image in Figure 5c shows the lattice at the edge of one of the main faces, revealing a spacing of 2.5 Å, which corresponds to Bragg diffraction precisely from 1/3{422} lattice planes.[19] In this image it can be also seen that near the edge, the crystalline structure presents almost no defects and the roughness of the edges is basically at an atomic scale. The HRTEM image shown in Figure 5d is a side view of two parallel triangles near their tips. The regularity and single-crystalline structure is obvious, with constant interplane distances and thicknesses. In Figures 5a and d it can be seen that the tips are almost perfect except for some curvature, which may slightly influence the ultimate optical response. It is also interesting to note that the HRTEM images in Figures 5c and d clearly show the amorphous PVP protective layer around the surfaces of the Ag particles, with a thickness usually ranging between 1 and 3 nm.

2.3. Growth of Nanoprisms via Illumination Through Filters

So far, we have shown solid evidence to claim that the size and shape of the particles (and, subsequently, their optical properties) are mainly determined by the wavelength of illumination, though other parameters such as temperature and the intensity of irradiation can also have some effect. To confirm this, additional experiments were performed using a photoreactor containing 16 fluorescent tubes. The emission spectrum of these lamps shows a broad band between 300 and 700 nm, with two sharp emission peaks at 436 and 546 nm (see Supporting Information). Apart from direct illumination with the fluorescent tubes, illumination conditions similar to those used in the experiments performed with LEDs were achieved by wrapping the samples with green- and red-

color filters and illuminating with the fluorescent tubes. The transmission spectra of the filters overlapped with the emission spectra of the photoreactor lamps as shown in the Supporting Information. In Figure 6, we show the result of subtracting the absorption spectrum of the filters from the emission spectrum of the lamps, compared to the emission spectra of the LEDs.

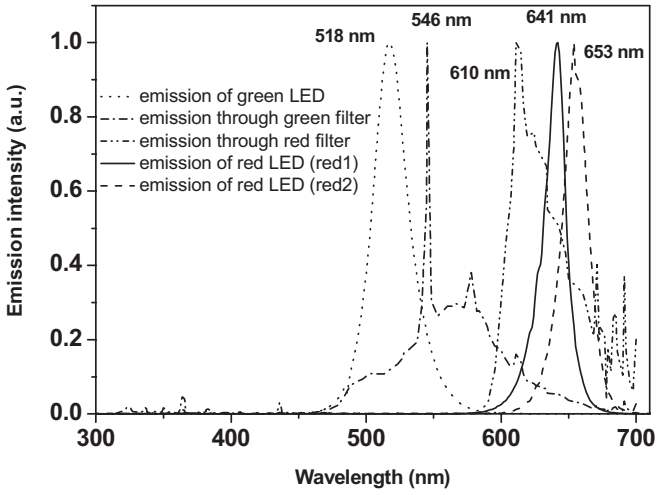

Figure 6. Normalized emission spectra of light emitted by fluorescent tubes after passing through green (–·–·–) and red (–··–··) filters, compared to the emission spectra of green (·····), red1 (–), and red2 (– – –) LEDs. The maximum wavelengths are indicated by the labels.

The result of using green and red filters is somehow similar to that using illumination with green and red LEDs, although we see clear shifts in the emission bands (518 and 546 nm for the green LED and filter, respectively; 610, 641, and 653 nm for the red filter and red1 and red2 LEDs, respectively). Thus, it will be interesting to compare the results of the two illumination systems, since they provide a systematic shift of the illumination wavelength between 518 and 653 nm. Additionally, the use of filters leads to red-shifted emission with respect to green LED but blue-shifted emission with respect to red LEDs, which is beneficial for a proper comparison.

Figure 7 shows the UV–vis–NIR spectra of the silver-nanoprism dispersions obtained through illumination of the starting Ag colloids within the photoreactor, both with no filter and with wrapping the sample with green and red filters. While direct illumination with the broad lamp emission led to a spectrum with the intense in-plane dipolar plasmon absorption centered at 642 nm (indicating formation of relatively small triangles), illumination through the green filter produced Ag nanoprisms with the main absorption at 1076 nm, and the main band of the sample wrapped with a red filter was located at 1294 nm. Although the main emission peaks of the photoreactor are located at 436 and 546 nm,

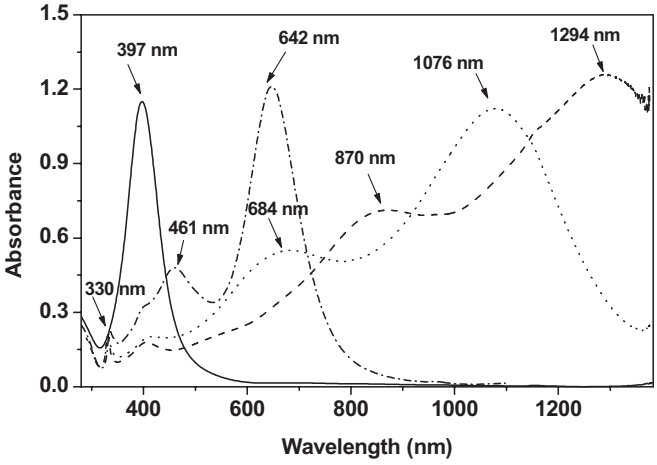

Figure 7. UV–vis–NIR spectra of dispersions of Ag seeds (–) and nanoprisms in water obtained using a photoreactor (–·–·–), and combining it with green (·····) and red (– – –) filters. The band maxima are indicated by the labels.

which, according to the model proposed by Jin et al. should yield a monomodal distribution, we find, again, a bimodal distribution, reflected in the intense secondary band at 461 nm, which is mainly due to the presence of smaller particles (mainly prisms), as confirmed by TEM (see Supporting Information). Again, we see that higher emission wavelengths lead to highly red-shifted in-plane dipole plasmon bands, and, thus, assuming that the particles have the same thickness (which was confirmed by SEM and TEM), to nanoprisms with higher aspect ratios. Additionally, the relative positions of the absorption bands correlate well with the relative positions of the emission bands shown in Figure 6. The particles illuminated through the green filter absorb at higher wavelengths than those obtained using green LEDs, while the particles illuminated through the red filter absorb at lower wavelengths than those obtained using red LEDs. The sizes of the obtained triangles were measured using TEM and correlate well with the expected trend (see Table 2), i.e., longer lateral sizes for samples illuminated at longer wavelengths.

Nevertheless, under "red conditions" particles produced using filters were smaller than nanoprisms obtained using LEDs. This was all confirmed by TEM (Table 2); the green filter led to particles with an average side length of 123 nm (110 nm in the case of green LEDs), while the red filter led to particles with an average side length of 174 nm (192 and 242 nm in the case of the red LEDs).

Table 2. Average side lengths and band maxima of Ag nanoprisms obtained under different illumination conditions.

Light source (emission wavelength [nm])	Green LEDs (518)	Green filter (546)	Red filter (610)	Red1 LEDs (641)	Red2 LEDs (653)
Main band maximum [nm]	1037	1076	1294	1385	1491
Average side length [nm]	110 ± 16.5	123 ± 25.1	174 ± 46.0	192 ± 39.2	242 ± 52.4

ADVANCED FUNCTIONAL MATERIALS

Besides the bands due to in-plane dipole plasmon resonances, the absorption spectra shown in Figure 7 display other bands at lower wavelengths (461, 684, and 870 nm for no filter, the green and the red filter, respectively), which again arise from in-plane dipole resonances of a second population of smaller particles. Absorption at 330 nm (a less-intense but well-defined peak) is also observed, which is due to out-of-plane quadrupole resonances.[4b] As usual, the out-of-plane dipole and in-plane quadrupole resonances cannot be clearly distinguished. It should also be noted that the bands are wider and less intense than those obtained using LEDs, probably because of the higher wavelength dispersion of the illumination when filters are used, and this is also reflected in a higher polydispersity of the nanoprisms, as determined by TEM (see Table 2).

Figure 8 summarizes the results obtained from the LED and filter experiments. We find a quasilinear correlation of the particle side length with the emission wavelength and the position of the in-plane dipole plasmon band. This is a clear demonstration that particle size can be tuned by controlling the illumination wavelength, without affecting the particle shape and thickness. Similar results have been reported by Jin et al. using lasers as the illumination source,[13c] but obtaining in-plane plasmon bands centered below 900 nm.

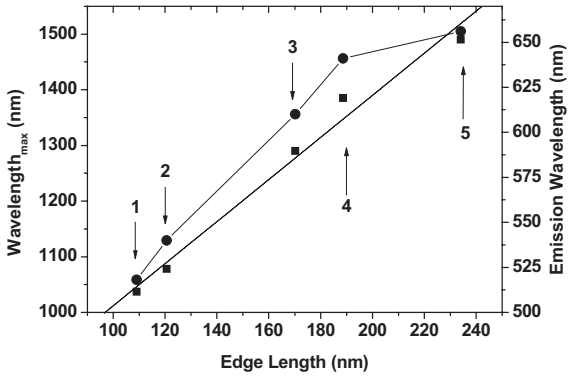

Figure 8. Average side length as a function of the position of the plasmon band (circles) and the emission wavelength of the illumination source (squares) for nanoprisms prepared by illumination with green LEDs (1), through a green filter (2), through a red filter (3), and with red1 (4) and red2 LEDs (5).

2.4. Influence of Temperature

The sphere-to-prism conversion is, in general, a slow process (typical reaction times of several days). However, both temperature and the intensity of the illumination source were found to affect the rate of the process. An increase from 25 to 37 °C was sufficient to reduce the time needed for completion (no further spectral changes) from 159 to 69 h when illumination was performed with green LEDs (working at 20 mA), and from 185 to 96 h for illumination with red LEDs (red2, working at 20 mA). However, the temperature increase did not affect either the final shape or size of the particles, and, thus, the final spectra obtained at room temperature and at 37 °C were very similar (see Supporting Information).

2.5. Mechanism

As previously reported,[13a] when the starting Ag colloid is stored in the dark, no conversion takes place. Additionally, illumination with NIR or UV light was observed to drive the aggregation of the Ag colloids to form larger, spherical particles. It is thus quite clear that the process of Ag-nanoprism formation is induced by visible light, and is mostly sensitive to the emission wavelength of the illumination source. However, despite some attempts to determine the mechanism of the process,[13c] there is still some controversy. Trying to shed some light on the mechanism, we carefully analyzed the spectral evolution during the reaction for the various illumination conditions, and combined it with the information about the nanoprism morphology obtained from electron microscopy. Figure 9 shows the evolution of UV–vis–NIR spectra during the formation of Ag nanoprisms using red LEDs (Fig. 9A) and white light combined with a red filter (Fig. 9B). To simplify the analysis of the spectra, we plotted in the corresponding insets the kinetic traces at 397 nm (maximum wavelength, λ_{max}, for the starting Ag colloids), 1330 and 890 nm (λ_{max} for the in-plane dipole bands of the two main nanoprism populations produced with red2 LEDs), and 1290 and 870 nm (λ_{max} for the in-plane dipole bands of the two main populations produced with the red filter). In each trace we can distinguish three different stages. In the initial stage nanoprism formation has not commenced, but there is an increase and a slight red-shift of

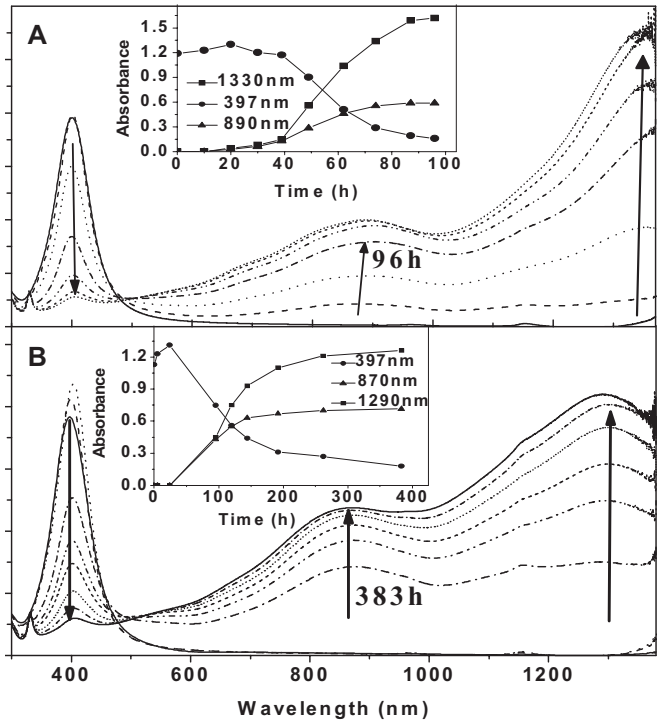

Figure 9. Time evolution of UV–vis–NIR spectra during the formation of Ag nanoprisms by illumination with red LEDs (A) and through a red filter (B). The insets show the evolution of the absorbance at the wavelength of the three main peaks as a function of the illumination time.

the band at 397 nm. TEM analysis (Fig. 10) provided evidence that, during this stage, larger particles were formed by aggregation of the small starting spherical particles. A similar process was observed by Callegari et al.,[13b] who claimed that this was due to weak attractive forces arising after the excess borohydride ions constituting the particle repulsive layer were photooxidized.

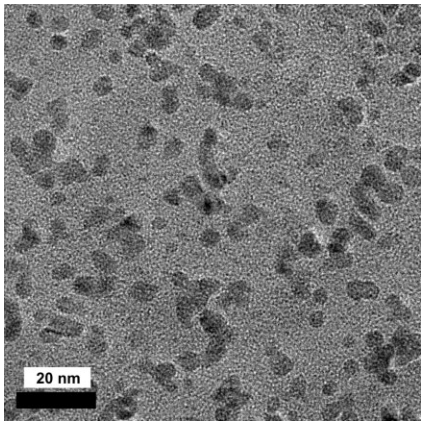

Figure 10. Representative TEM image of the process of Ag-seed aggregation during sample illumination with red LEDs.

Once such larger particles are present, an intermediate stage starts where the band at 397 nm drops (original Ag seeds are consumed) and two new bands appear, corresponding to in-plane resonances of the two main populations of silver nanoprisms. Both processes start basically at the same irradiation time, suggesting that they are correlated, i.e., the nanoprisms are formed by consumption of the original Ag seeds. This statement is supported by two further observations: almost no shift of the low-energy bands during the reaction (just a steady increase in intensity); and the presence of an isosbestic point at approximately 490 nm (observed in all experiments, see Fig. 9). These results rule out mechanisms such as Ostwald ripening (even at short reaction times the nanoprisms are well defined) as well as fusion of intermediate prisms (extensive TEM analysis during different stages of the process did not reveal the presence of dimer or trimer intermediates). Additionally, since Ostwald ripening is almost temperature insensitive (within the range considered here), the observed increase in reaction rate with temperature agrees with the previous statement, and suggests that collisions between particles play an important role. The continuous decrease in the concentration of small particles and early formation of large nanoprisms suggests that a well-defined final optimum size exists for each particular illumination condition, which is achieved through aggregation of small silver spheres (Fig. 10). One aspect that has been recently pointed out by Sun and Xia[13f] is the importance of the presence of sodium citrate during irradiation, suggesting that a combination of chemical and photochemical processes can be involved for the sphere-to-prism conversion.

3. Conclusions

Anisotropic silver nanoprisms with strong absorption in the NIR region can be synthesized by illumination of small silver-nanoparticle seeds with low-intensity LEDs or white light combined with color filters. The observed quasilinear dependency of particle size on the illumination wavelength, regardless of the nature of the light source, indicates that the final nanoprism size can be tuned by controlling the illumination conditions, without affecting the shape and thickness of the particles. We propose a mechanism based on the formation of the Ag nanoprisms via the consumption of the preformed Ag seeds, which is different from other mechanisms previously proposed by others.

4. Experimental

Chemicals: Sodium borohydride ($NaBH_4$, 99 %), silver nitrate ($AgNO_3$, 99+ %), and sodium chloride (NaCl, ≥ 99 %) were purchased from Aldrich. Trisodium citrate dihydrate (98 %) was purchased from Sigma and poly(vinylpyrrolidone) (PVP, weight-average molecular weight, $M_W = 10\,000$ kg mol^{-1}), from Fluka. MilliQ deionized water (resistivity higher than 18 MΩ cm) was used for all preparations. All chemicals were used without further purification.

Preparation of Silver Nanoprisms: Small silver nanoparticles were prepared as previously reported [8c]. Briefly, 200 mL 0.1 mM $AgNO_3$ solution was reduced with 2 mL 0.5 mM $NaBH_4$ in the presence of trisodium citrate (0.3 mM) under gentle stirring. Immediately after injection of the reducing agent, 2 mL of a 5 wt % aqueous solution of PVP was added.

Growth of Nanoprisms via Illumination with LEDs: The experimental setup consisted of a dark box with four LEDs that entered the lateral walls and were connected to a standard power supply. Emission spectra and other operation parameters of the LEDs used are shown in the Supporting Information and in Table 1. The Ag-seed solution was placed within a quartz cuvette (10 mm path length) in the center of the box, at a distance of 2.5 cm from each LED. The temperature inside the dark box was 25 ± 2 °C. The experiments at 37 °C were performed inside an oven (Memmert, ULE 400).

Growth of Nanoprisms via Illumination through Filters: The experiments were carried out inside a commercial photoreactor (Luzchem LZC-Vis) containing 16 Sylvania cool-white fluorescent tubes (300 nm < λ < 700 nm, 8 W). To change the illumination conditions, the samples (20 mL) were wrapped with green or red plastic filters (e-color+, Rosco) (transmission spectra are included in the Supporting Information). The distance from the sample to the fluorescent tube was 3 cm. The temperature inside the photoreactor was 30 ± 2 °C.

Characterization: A JEOL JEM 1010 transmission electron microscope operating at an acceleration voltage of 100 kV was used for low-magnification imaging, while HRTEM images were obtained using a JEOL JEM 2010 FEG-TEM operating at an acceleration voltage of 200 kV. SEM characterization was carried out using a JEOL JSM-6700F FEG-SEM operating at an acceleration voltage of 5 kV for secondary-electron imaging (SEI) and at 20 kV for backscattering-electron imaging (YAG detector).

UV–vis–NIR spectra were measured using a Cary 5000 UV–vis–NIR spectrophotometer. Samples requiring measurements above 1350 nm were centrifuged and redispersed in D_2O to avoid absorption contribution from H_2O.

Received: September 28, 2005
Final version: January 9, 2006
Published online: March 13, 2006

ADVANCED FUNCTIONAL MATERIALS

[1] a) K. E. Drexler, C. Peterson, G. Pergamit, *Unbounding the Future: The Nanotechnology Revolution* Morrow, New York **1991**. b) *Springer Handbook of Nanotechnology* (Ed: B. Bhushan), Springer, Berlin **2004**. c) *Introduction to Nanotechnology* (Eds: C. P. Poole, Jr., F. J. Owens), John Wiley & Sons, New York **2003**. d) *Nanoscale Materials* (Eds: L. M. Liz-Marzán, P. V. Kamat), Kluwer Academic, Boston, MA **2003**.

[2] a) A. J. Haes, D. A. Stuart, S. Nie, R. P. Van Duyne, *J. Fluoresc.* **2004**, *14*, 355. b) R. E. Bailey, A. M. Smith, S. Nie, *Phys. E* **2004**, *25*, 1.

[3] *Optical Properties of Metal Clusters* (Eds: U. Kreibig, M. Vollmer), Springer, Berlin **1995**.

[4] a) E. Hao, G. C. Schatz, J. T. Hupp, *J. Fluoresc.* **2004**, *14*, 331. b) K. L. Kelly, E. Coronado, L. L. Zhao, G. C. Schatz, *J. Phys. Chem. B* **2003**, *107*, 668. c) V. Germain, A. Brioude, D. Ingert, M. P. Pileni, *J. Chem. Phys.* **2005**, *122*, 124 707. d) A. Brioude, M. P. Pileni, *J. Phys. Chem. B* **2006**, *22*, 32. e) L. M. Liz-Marzán, *Langmuir* **2005**, *109*, 21 159.

[5] a) A. J. Haes, R. P. Van Duyne, *J. Am. Chem. Soc.* **2002**, *124*, 10 596. b) Y. Sun, Y. Xia, *Anal. Chem.* **2002**, *74*, 5297.

[6] a) R. A. Shelby, D. R. Smith, S. Schultz, *Science* **2001**, *292*, 77. b) S. A. Maier, M. D. Friedman, P. E. Barclay, O. Painter, *Appl. Phys. Lett.* **2005**, *86*, 071 103.

[7] a) E. Hao, G. C. Schatz, *J. Phys. Chem. B* **2004**, *108*, 357. b) J.-M. Nam, C. S. Thaxton, C. A. Mirkin, *Science* **2003**, *301*, 1884.

[8] I. O. Sosa, C. Noguez, R. Barrera, *J. Phys. Chem. B* **2003**, *107*, 6269.

[9] a) M. Maillard, S. Giorgio, M. P. Pileni, *Adv. Mater.* **2002**, *14*, 1084. b) C. Salzemann, J. Urban, I. Lisiecki, M. P. Pileni, *Adv. Funct. Mater.* **2005**, *15*, 1277.

[10] a) B. Nikoobakht, M. A. El-Sayed, *Chem. Mater.* **2003**, *15*, 1957. b) Y. Xia, P. D. Yang, Y. G. Sun, Y. Y. Wu, B. Mayers, B. Gates, Y. D. Yin, F. Kim, Y. Q. Yan, *Adv. Mater.* **2003**, *15*, 353. c) J. Pérez-Juste, L. M. Liz-Marzán, S. Carnie, D. Y. C. Chan, P. Mulvaney, *Adv. Funct. Mater.* **2004**, *14*, 571. d) N. R. Jana, L. Gearheart, C. J. Murphy, *Chem. Commun.* **2001**, 617.

[11] a) N. Malikova, I. Pastoriza-Santos, M. Schierhorn, N. A. Kotov, L. M. Liz-Marzán, *Langmuir* **2002**, *18*, 3694. b) J. E. Millstone, S. Park, K. L. Shuford, L. Qin, G. C. Schatz, C. A. Mirkin, *J. Am. Chem. Soc.* **2005**, *127*, 5312. c) F. Kim, S. Connor, H. Song, T. Kuykendall, P. Yang, *Angew. Chem. Int. Ed.* **2004**, *43*, 3673. d) S. S. Shankar, A. Rai, B. Ankamwar, A. Singh, A. Ahmad, M. Sastry, *Nat. Mater.* **2004**, *3*, 482.

[12] a) I. Pastoriza-Santos, L. M. Liz-Marzán, *Nano Lett.* **2002**, *2*, 903. b) S. Chen, D. L. Carroll, *Nano Lett.* **2002**, *2*, 1003. c) S. Chen, D. L. Carroll, *J. Phys. Chem. B* **2004**, *108*, 5500. d) N. Okada, Y. Hamanaka, A. Nakamura, I. Pastoriza-Santos, L. M. Liz-Marzán, *J. Phys. Chem. B* **2004**, *108*, 8751. e) G. S. Métraux, C. A. Mirkin, *Adv. Mater.* **2005**, *17*, 412.

[13] a) R. Jin, Y. W. Cao, C. A. Mirkin, K. L. Kelly, G. C. Schazt, J. G. Zheng, *Science* **2001**, *294*, 1901. b) A. Callegari, D. Tonti, M. Chergui, *Nano Lett.* **2003**, *3*, 1565. c) R. Jin, C. Y. Cao, E. Hao, G. Métraux, G. C. Schazt, C. A. Mirkin, *Nature* **2003**, *425*, 487. d) M. Maillard, P. Huang, L. E. Brus, *Nano Lett.* **2003**, *3*, 1611. e) Y. Sun, B. Mayers, Y. Xia, *Nano Lett.* **2003**, *3*, 675. f) Y. Sun, Y. Xia, *Adv. Mater.* **2003**, *15*, 695.

[14] a) A. J. Haes, J. Zhao, S. Zou, C. S. Own, L. D. Marks, G. C. Schatz, R. P. Van Duyne, *J. Phys. Chem. B* **2005**, *109*, 11 158. b) X. Zhang, E. M. Hicks, J. Zhao, G. C. Schatz, R. P. Van Duyne, *Nano Lett.* **2005**, *5*, 1503.

[15] C. Loo, A. Lowery, N. Halas, J. West, R. Drezek, *Nano Lett.* **2005**, *5*, 709.

[16] a) P. Boire, F. Didier, J.-M. Grima, *US Patent 6 582 809*, **2001**. b) N. R. Lynam, *US Patent 5 523 877*, **1996**.

[17] A. I. Kirkland, D. A. Jefferson, D. G. Duff, P. P. Edwards, *Inst. Phys. Conf. Ser.* **1990**, *98*, 375.

[18] C. Lofton, W. Sigmund, *Adv. Funct. Mater.* **2005**, *15*, 1197.

[19] A. I. Kirkland, D. A. Jefferson, D. G. Duff, P. P. Edwards, I. Gameson, B. F. G. Johnson, D. J. Smith, *Proc. R. Soc. London Ser. A* **1993**, *440*, 589.